Parabolic microlensed optical fiber for coupling efficiency improvement in single mode fiber

Zaied Bouhafs, Assia Guessoum, Abdelhak Guermat, Djamila Bouaziz, Sylvain Lecler, Nacer-Eddine Demagh

Research Article Vol. 1, No. 5 / 15 May 2022 / Optics Continuum 1218
OPTICS CONTINUUM

Parabolic microlensed optical fiber for coupling efficiency improvement in single mode fiber

ZAIED BOUHAFS,[1] ASSIA GUESSOUM,[1] ABDELHAK GUERMAT,[1] DJAMILA BOUAZIZ,[1,2,3] SYLVAIN LECLER,[2,3] AND NACER-EDDINE DEMAGH[1,*]

[1]LOA, IOMP, Ferhat Abbas University Setifl, Setif 19000, Algeria. LOA, IOMP, Université Sétif 1, Algeria
[2]ICube, University of Strasbourg, UMR CNRS 7357 - Illkirch 67412, France
[3]INSA de Strasbourg, Strasbourg, France
*ndemagh@univ-setif.dz

Abstract: The efficiency of optical coupling between an optical fiber and other components be it a light source, a photodetector or another fiber, often depends on the performance of the focusing components. In optoelectronics, microlenses are generally incorporated at the end of optical fibers to ensure optimal coupling. These microlenses are primarily fabricated with a spherical profile easier to achieve, with a determined radius and at low production costs. However, these microlenses exhibit a relatively large waist due to intrinsic spherical aberrations making it difficult to couple light into single mode fibers. This paper presents the results of a study of a microlens having a parabolic profile that has been made of polydimethylsiloxane (PDMS) at a single mode optical fiber (SMF 9/125) end terminal. The contribution of the parabolic profile as compared to spherical shaped one is analyzed. Estimates at the wavelengths of primary importance, λ =1.310 µm and λ =1.550 µm, have shown a decrease in the spot radius diagram in the focal plane by 3, from an root mean square (RMS) value of 0.623 µm in the spherical case to less than 0.229 µm in the parabolic case. The measured optical coupling has improved to 98.5% under optimal conditions (without taking into account the bulk absorption and the effects of Fresnel reflection). For different studied microlens curvatures' radii, the obtained waist values vary from 1.00 to 4.90 µm with working distances from 5.80 to 48.80 µm, respectively.

1. Introduction

Owing to facts such that the minimum of silica-based single mode optical fibers (SMF) dispersion occurring at the wavelength of approximately 1.300 µm and the zero-dispersion wavelength, towards the minimum-loss window at approximately 1.550 µm, this study is carried out in both wavelengths 1.310 and 1.550 µm, these are prevalent in optical communication systems.

Effective coupling between laser diode sources (LD) and single mode fibers or other optical components is an essential requirement in many applications, particularly in optical communication systems involving optical fiber connections. The propagation of light should then be properly collimated using appropriate microlenses. The latter are usually spherical with a simple geometric shape that can be described by a constant curvature radius. Various studies have been conducted on micro-collimators embedding spherical and hemispherical microlenses [1–4]. Although these microlenses are simple to manufacture and of low cost, their performance is affected by induced spherical aberrations. These defects, inherent to their geometry, are at the origin of the focusing spot widening. To avoid these aberrations, aspherical structures with non-constant bending radii are employed; the complex shape of the microlenses allows for the correction of spherical aberrations. In this case, the profiles are more complex and can be described analytically by a curvature radius that is constituted of several terms of higher order coefficients. The estimate of the first term of the series shows, as for classical lens, that the

#441633 https://doi.org/10.1364/OPTCON.441633
Journal © 2022 Received 20 Sep 2021; revised 27 Jan 2022; accepted 28 Jan 2022; published 11 May 2022

OPTICS CONTINUUM

parabolic microlens is a prime candidate to be added to optical fibers. This ensures a better coupling efficiency.

To correct aberrations and optimize light transfer, various aspherical microlenses were investigated, essentially elliptical, conical, hyperbolic and parabolic. Aspherical plano-convex lenses have been used to correct aberrations that would be produced by an equivalent conventional lens [5]. While a biconvex structure made up of two microlenses was proposed [6], the result in reducing aberrations was not as good as in the aspherical shaped case. Nevertheless, the use of elliptical microlenses was reported to give a high coupling rate [7]. These structures are more suitable when it comes to coupling light from an axially non-symmetrical source to optical fibers. They compensate for the beam asymmetry but not for correcting aberrations. It has been reported that an increase in the coupling rate between a LD source and a truncated conical microlens micro-collimator was obtained [8] and in which only the multiple reflections between the two components' surfaces have been considered. A comparative study on the coupling efficiency between two single mode fibers (SMF) using spherical, conical and graded index (GRIN) rod microlenses carried out under optimal conditions gave a coupling efficiency higher than 91% for the spherical microlens case [9]. It was lower in comparison to other microlenses, yet, it was less sensitive to angular misalignment (Tilt). Aberrations remained the main reason for its coupling weakness. Microlenses with hyperbolic profiles have been proposed to reducing aberrations' effects [10–11]. The focusing spots widths were smaller than those obtained using spherical lenses with the same characteristics. A concept based on a planar type microlens of a multilayer design that relies on depositing a doped polymer of varying refractive indices on a concave surface was also proposed [12]. This has enabled to reduce spherical aberrations by correcting the light path. Narrow focusing properties through combining a GRIN and a glass hemispherical microlens have also been reported [13–14]. Recently, a report has been published on the use of sub-wavelength photonic nano-jet focusing [15], but this has required the use of large mode area fiber.

All these reported studies, in general, aim at improving the coupling efficiency; as such, the introduction of calculations based on the ABCD matrix transformation method has simplified evaluating of the coupling efficiency. This was widely adopted in optical fibers that included microlenses. The latter process different profiles and, in particular, the parabolic profile [16] where it was reported that coupling efficiency could reach 100% under optimal conditions (neglecting internal reflections).

In this work, the results of the study are presented on the characteristics and performance of an SMF optical fiber (9/125 μm) microlens that we have elaborated having a parabolic profile [17]. The latter has been made of PDMS (Sylgard 184) that is increasingly used in the fabrication and prototyping of optical systems and so on. The optical propagation behavior through the microlens has been computed using the ABCD transformation matrix method, which allowed us to determine its main characteristics such as the focus waist and the working distance. It is shown that such parabolic microlens offers better coupling performance as compared to microlenses with an equivalent hemispherical shape.

2. Characterization and analysis of aberration

The optical system shown in Fig. 1 is considered. It is composed of an SMF having a parabolic microlens of refractive index n_s and a radius of curvature R at the apex. We analyzed the light propagation behavior through the microlens in order to determine parameters of interest of the transmitted beam, for instance, the waist w_1 and the working distance Z.

The beam propagation path undertaken through the microlens is as indicated in Fig. 1. The wave guided by the SMF mode width fiber $2w_0$ is projected by the microlens into a waist image

OPTICS CONTINUUM

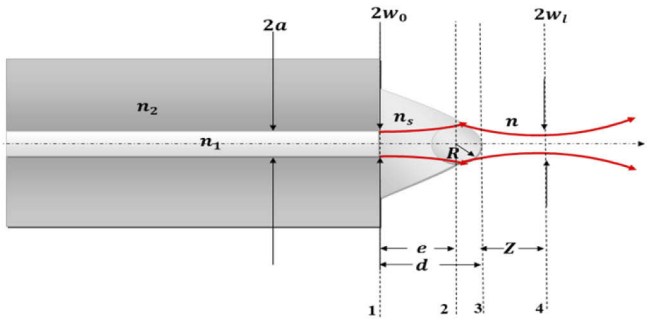

Fig. 1. Light propagation through the microlens.

w_l.The mode width $2w_0$ is determined using Marcuse relation [18]:

$$\frac{w_0}{a} = 0.65 + \frac{1.619}{V^{3/2}} + \frac{2.879}{V^6} \tag{1}$$

where a is the core radius of the SMF, i.e. a = 4.5 μm for 9/125 μm fiber, and V is the normalized frequency given by the relation:

$$V = \frac{2\pi}{\lambda} a \sqrt{n_1^2 - n_2^2} \tag{2}$$

with n_1 and n_2 being the core and cladding indices, respectively, and λ is the free-space wavelength used, λ =1.31 μm. The estimate gives $w_0 = 4.1$ μm.

The calculation of the mode field width $2w_0$ allows the determination of other optical characteristics, such the new waist w_l and the working distance Z, by using the transfer matrix M of the optical system. This matrix can be broken down into 3 elementary matrices corresponding to the different propagation media. It is written as:

$$M = M_{34} M_{23} M_{12} \tag{3}$$

where M_{12}, M_{23} and M_{34} are the transfer matrices, respectively, of the propagation medium between planes 1 and 2, of the parabolic microlens between planes 2 and 3, and that of the image waist formation medium between planes 3 and 4 in air with an index n_0. By considering the ABCD law, the following equation is obtained [19]:

$$M = \begin{pmatrix} A & B \\ C & D \end{pmatrix} = \begin{pmatrix} 1 & Z \\ 0 & 1 \end{pmatrix} \begin{pmatrix} 1 & 0 \\ \frac{n_0 - n_s}{n_0\, p} & \frac{n_s}{n_0} \end{pmatrix} \begin{pmatrix} 1 & \frac{d}{n_s} \\ 0 & 1 \end{pmatrix} \tag{4}$$

with

$$M_{12} = \begin{pmatrix} 1 & \frac{d}{n_s} \\ 0 & 1 \end{pmatrix} \tag{5}$$

$$M_{23} = \begin{pmatrix} 1 & 0 \\ \frac{n_0 - n_s}{n_0\, p} & \frac{n_s}{n_0} \end{pmatrix} \tag{6}$$

$$M_{34} = \begin{pmatrix} 1 & Z \\ 0 & 1 \end{pmatrix} \tag{7}$$

where d is the thickness of the microlens and p is the focal parameter of the parabolic profile. The apex can be described by an inscribed circle of radius $R = p$ [20].

OPTICS CONTINUUM

From Eq. (4), the parameters A, B, C and D can be deduced as follows:

$$A = 1 + Z\left(\frac{n_0 - n_s}{n_0\, R}\right) \tag{8}$$

$$B = \frac{d}{n_s} + \frac{d}{n_s} Z\left(\frac{n_0 - n_s}{n_0\, R}\right) + Z\frac{n_s}{n_0} \tag{9}$$

$$C = \frac{n_0 - n_s}{n_0\, R} \tag{10}$$

$$D = \frac{d}{n_s}\frac{n_0 - n_s}{n_0\, R} + \frac{n_s}{n_0} \tag{11}$$

The new waist w_l and the working distance Z [21] are deduced from Eq. (12) and (13) as follows:

$$AC + g^2 BD = 0 \tag{12}$$

$$w_l = w_0\left(\frac{n_s}{n_0}\frac{A^2 + g^2 B^2}{AD - BC}\right)^{1/2} \tag{13}$$

where

$$g = \frac{\lambda}{\pi w_0^2 n_s} \tag{14}$$

By solving the previous equations, the working distance Z and the waist w_l are deduced which take the following relations:

$$Z = -\frac{1 + g^2 d\left(\frac{d}{{n_s}^2} + \frac{R}{1-n_s}\right)}{\frac{1-n_s}{R} + g^2 d\left(\frac{d}{{n_s}^2}\frac{1-n_s}{R} + 2 + \frac{{n_s}^2}{d}\frac{R}{1-n_s}\right)} \tag{15}$$

$$w_l = w_0\left(1 + \frac{g^2 d^2}{{n_s}^2} + \frac{g^2 dZ(1-n_s)}{R}\left[\frac{2}{g^2 d} + \frac{2d}{{n_s}^2} + \frac{2R}{1-n_s} + Z\left(\frac{1-n_s}{g^2 dR} + 2 + \frac{d(1-n_s)}{{n_s}^2 R} + \frac{{n_s}^2 R}{d(1-n_s)}\right)\right]\right)^{1/2} \tag{16}$$

2.1. Characterization of the microlens profile

Figure 2 shows a magnified view of a typical polydimethylsiloxane (PDMS) parabolic microlens attached to the end of an SMF optical fiber (9/125 µm) with refractive index of core, respectively, is 1.4675 at 1.310 µm and 1.4681 at 1.550 µm. A numerical aperture of 0.12 and a relative refractive index difference of 0.36%.

The profile of the microlens is determined by image processing. Indeed, starting from the experimental image in Fig. 2 (a), the coordinates of the points of the microlens contour are extracted and represented by the points as shown in Fig. 2 (b).

These points are then interpolated by a function of the form $y = ax^b$ to determine its profile. The parameters (a and b) are determined by power regression. The calculations yielded the following values:

$a = 0.0277$

$b = 2.1153$

with a residual of 1.0×10^{-13}.

Then, the profile equation follows:

$$y = 0.0277\, x^{2.1} \tag{17}$$

Figure 2(b) shows the experimental points and the parabolic interpolation curve.

OPTICS CONTINUUM

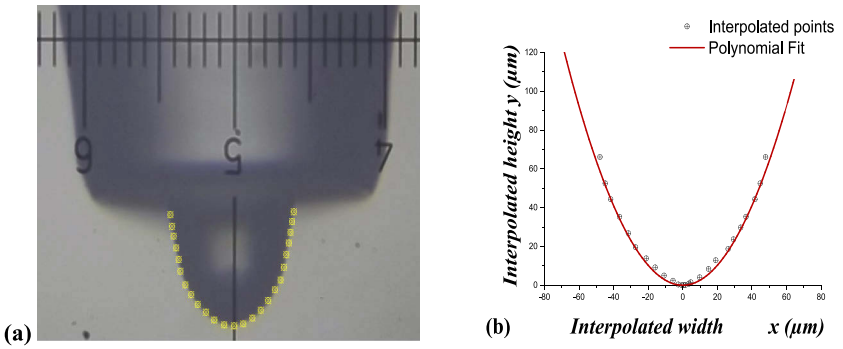

Fig. 2. (a) Profile of the parabolic microlens at the end of a fiber (SMF 9/125). Height (thickness) of 50 µm, base width of 54 µm and bending radius $R = 17.5$µm. Dots (●●●) extraction of the contour points of the parabolic microlens and (b) representation of the experimental points of the microlens contour and the continuous line interpolation function.

2.2. *Correction of spherical aberrations by a parabolic microlens*

A spherical aberration is an aperture defect which results from the lens spherical shape. The light rays coming from a point at infinity are deflected differently according to their distance from the optical axis. The furthest rays from the optical axis converge more than the paraxial rays, which leads to the appearance of different image foci on the optical axis.

The spherical aberration, thus, appears in two dimensions: along the optical axis with different image focal points, and around the optical axis with diffraction spots of different diameters. This is why two types of spherical aberrations can be distinguished. The longitudinal spherical aberration is equivalent to the distance between the marginal focus and the paraxial focus on the one hand, and on the other one, the transverse spherical aberration, which measures the radius of the diffraction spot at the paraxial focus. One of the usual strategies to correct these aberrations is the use of a parabolic profile. Indeed, the latter was reported to be effective in minimizing these aberrations [22].

The aspherical surface schematized in Fig. 3, can be represented by parameters based on geometric equations, namely a radius of curvature R at the apex and a radial distance r varying radially from the center to the edge.

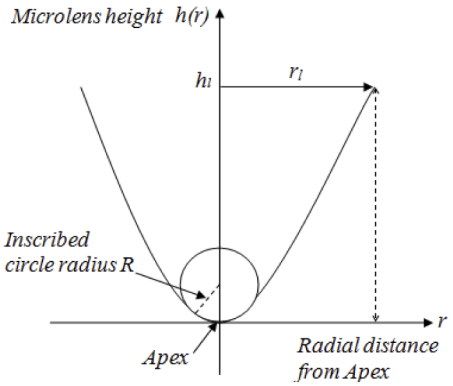

Fig. 3. Diagram of an aspherical surface.

OPTICS CONTINUUM

This profile is described by the function $h(r)$, which represents the height of the aspherical microlens as a function of the radial distance r to the optical axis. It is expressed as follows [23]:

$$h(r) = \frac{1}{R}\frac{r^2}{1+\sqrt{1-(1+K)\frac{r^2}{R^2}}} + A_4\, r^4 + A_6\, r^6 + A_8\, r^8 + \ldots \tag{18}$$

where A_i are constants calculated and given according to the geometric profile and parameters of the desired microlenses.

K is the aspheric constant [24]. The lens profile $h(r)$ is considered as spherical if ($K = 0$), elliptic if ($-1 < K < 0$ or $K > 0$), hyperbolic if ($K < -1$) and parabolic if ($K = -1$). The latter is of concern in this work.

In this study, the value of the aspheric constant K in the case of spherical, hyperbolic and parabolic microlenses is 0, -0.88 and -1, respectively.

The curvature radius at the vertex is given by the expression forthcoming,

$$R = (K+1)\frac{h_l}{2} + \frac{{r_l}^2}{2h_l} \tag{19}$$

where h_l is the height of the microlens and r_l is the radial distance to the optical axis at height h_l.

The back focal length of a plano-convex refractive lens is given by:

$$f = \frac{R}{n-1} = \frac{1}{2(n-1)}\left((K+1)\,h_l + \frac{r_l^2}{h_l}\right) \tag{20}$$

where n is the refractive index of the microlens.

The spherical aberration coefficient of a microlens is given by [25,26]:

$$S = (ON)^4 f \frac{n^2}{(n-1)^2} \tag{21}$$

where $ON = r/f$ represents the numerical aperture.

Then, the spherical aberration coefficients of a spherical microlens S_{sph}, parabolic microlens S_{par} and hyperbolic S_{hyp} are written, respectively, as follows:

$$S_{sph} = (ON)^4\left(\frac{h_l}{2} + \frac{{r_l}^2}{2h_l}\right)\frac{n^2}{(n-1)^3} \tag{22}$$

$$S_{par} = (ON)^4\left(\frac{{r_l}^2}{2h_l}\right)\frac{n^2}{(n-1)^3} \tag{23}$$

$$S_{hyp} = (ON)^4\left(\frac{K+1}{2}h_l + \frac{{r_l}^2}{2h_l}\right)\frac{n^2}{(n-1)^3} \tag{24}$$

The difference in the correction of spherical aberrations between these microlenses is estimated in terms of improvement D, by the following expressions:

$$D_{par} = \left(1 - \frac{S_{par}}{S_{sph}}\right) \tag{25}$$

$$D_{hyp} = \left(1 - \frac{S_{hyp}}{S_{sph}}\right) \tag{26}$$

Table 1 shows, for the same curvature radii, the aberration coefficients, S_{sph} of the spherical microlenses (Eq. 22), S_{par} of the studied parabolic microlenses (Eq. 23) and S_{hyp} of the hyperbolic microlenses (Eq. 24).

Table 1. Comparison Between Aberration Values of the Parabolic and Hyperbolic Shape Microlenses and the Hemispherical Ones Having the Same Curvature Radius and Refractive Index.

	$S_{Sph}(\mu m)$		$S_{Par}(\mu m)$		$S_{Hyp}(\mu m)$		$ImprovementD_{Par}(\%)$		$ImprovementD_{Hyp}(\%)$		$(D_{Hyp} - D_{Par})(\%)$	
R(μm)	λ=1.31 μm	λ=1.55 μm	λ=1.31 μm	λ=1.55 μm	λ=1.31 μm	λ=1.55 μm	λ=1.31 μm	λ=1.55 μm	λ=1.31 μm	λ=1.55 μm	λ=1.31μm	λ=1.55 μm
2.5	0.80	0.79	0.43	0.42	0.39	0.39	46.75	46.80	50.37	50.44	3.62	3.64
9.5	0.62	0.62	0.23	0.22	0.19	0.19	63.24	63.77	68.06	68.44	4.29	4.67
13.5	0.74	0.73	0.33	0.32	0.29	0.29	55.43	55.56	59.65	59.94	4.22	4.38
17.5	0.99	0.98	0.55	0.55	0.53	0.53	44.13	44.16	46.15	46.09	2.02	1.93
21.0	1.48	1.47	0.92	0.92	0.89	0.89	37.75	37.87	39.71	39.83	1.96	1.96

OPTICS CONTINUUM

The aberration minimums $S_{par} = 0.225\,\mu m$ and $S_{hyp} = 0.196$ were achieved at an optimal curvature radius $R = 9.5\,\mu m$ (at λ=1.550 µm). As a result, using the relations (Eq. 25) and (Eq. 26), the improvement in D by ~ 64% and 68% were achieved, respectively, in the case of parabolic and hyperbolic microlens shapes. Nevertheless, the difference between both results does not exceed 5%.

The corresponding variation curves are shown in Fig. 4(a) and 4(b). It is seen that the aberrations are much lower for parabolic and hyperbolic microlenses on the one hand while on the other hand their values are relatively close at both wavelengths 1.310 and 1.550 µm. Figure 4(c) and 4(d) show the improvement provided by parabolic and hyperbolic lenses. One can see that at the two relevant wavelengths the improvements are relatively close.

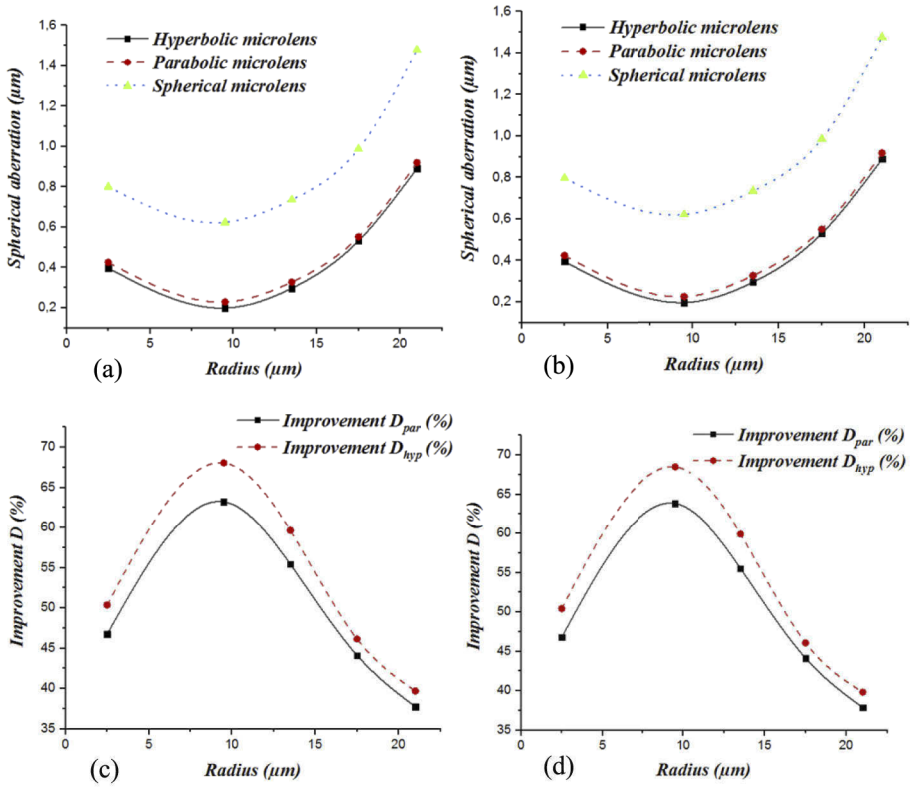

Fig. 4. (a)and (b) illustrate the spherical aberrations as a function of the curvature radii of spherical, parabolic and hyperbolic microlenses at λ=1.310 µm and λ=1.550 µm. (c) and (d)plot the improvement D_{par} and D_{hyp} of parabolic and hyperbolic microlenses as compared to their equivalent spherical ones.

The spherical aberrations cause a broadening of the spot diagram. For this purpose an Optics Software for Layout and Optimization (OSLO) is used. The latter designs, analyzes optical systems, evaluates performance and performs optimization and tolerance analysis. To check on this, the spot diagrams obtained by OSLO simulations are shown in Fig. 5(a, b, c) and in (d, e, f), respectively, at λ=1.310 µm and λ=1.550 µm. At the optimal wave length 1.550 µm, this results in an RMS geometric radius of the spot diagram of 0.225 µm for the parabolic case and 0.196 for the hyperbolic shape, respectively, around 2.8 and 3.1 times smaller than that of the spherical case with an RMS radius of 0.621.

OPTICS CONTINUUM

at λ=1.310 μm

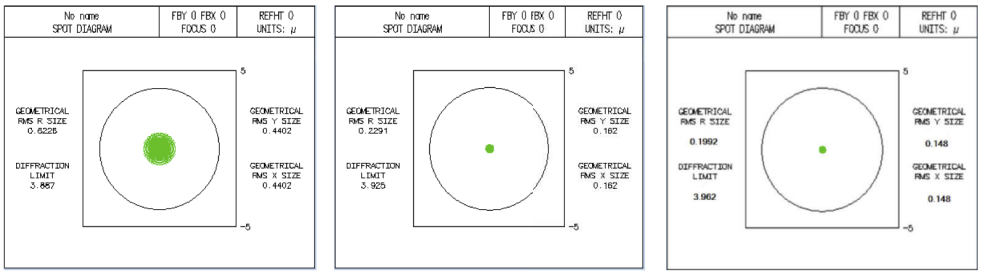

(a) Spherical microlens aberration (b) Parabolic microlens aberration (c) Hyperbolic microlens aberration

at λ=1.550 μm

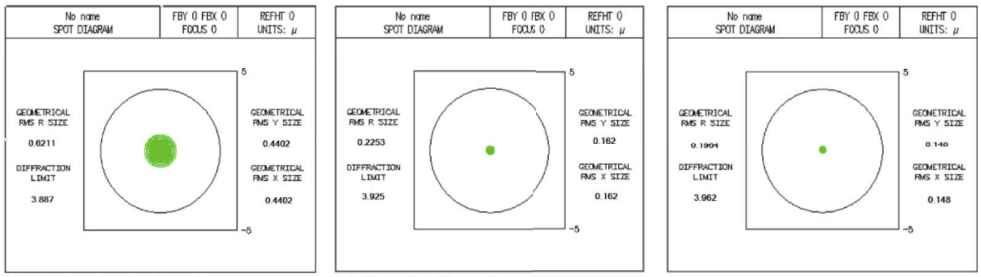

(d) Spherical microlens aberration (e) Parabolic microlens aberration (f) Hyperbolic microlens aberration

Fig. 5. The plot of the spot images, the case of $R = 9.50\,\mu m$. In (a), (b) and (c), respectively, the spot size for the spherical, parabolic and hyperbolic microlenses at λ=1.310 μm and in (d), (e) and (f) at λ=1.550 μm.

By considering the different spots' diameters, the parabolic and hyperbolic microlenses offer relatively a similar performance. There is a difference varying between them of 9.7% and 0%.

3. Calculation of the coupling efficiency and optimization of the bending radius of the microlenses

The coupling efficiency between a source and a fiber, via a parabolic microlens, placed at the end of the fiber is given [27] by the following integral:

$$\eta = \frac{\left|\iint \psi_r \psi_f^* dxdy\right|^2}{\iint |\psi_r|^2 dxdy \iint |\psi_f|^2 dxdy} \tag{27}$$

where Ψr and Ψ_f represent, respectively, the field of the beam transformed by a microlens and the mode field of the cleaved SMF optical fiber.

Figure 6 shows the coupling between two Gaussian beams, one with a waist w_l and a wave curvature radius R_l emanating from a 9/125 SMF with a microlens; the other is the $2w_f$ mode diameter of a cleaved SMF 4/125, where R_f is its wave curvature radius. The distance between the two waists is L.

OPTICS CONTINUUM

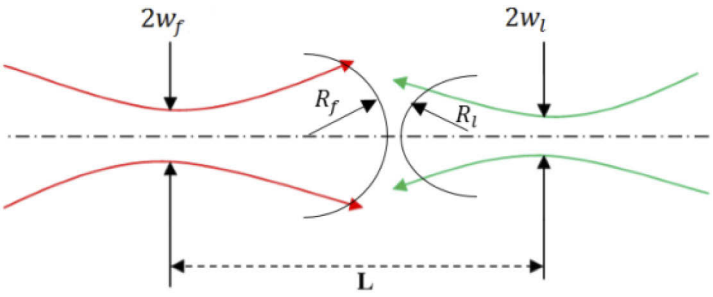

Fig. 6. Coupling between two Gaussian beams, in which the light beam propagates from left to right.

In this case, the coupling efficiency η is expressed in a simple form [28], given by the relation:

$$\eta = \frac{2w_f w_l}{\sqrt{\left(w_f^2 + w_l^2\right)^2 + \frac{\lambda^2 L^2}{\pi^2}}} \tag{28}$$

To evaluate the coefficient η, w_f and w_l are needed. The radius (waist) of the mode of the 4/125 µm cleaved fiber is calculated from Marcuse equation, i.e. w_f =2.28 µm, w_l of the microlens is experimentally determined in what follows.

4. Experimental set-up for characterizing the microlens

4.1. Determination of the waist and of the working distance

The experimental characterization consists of determining the optical parameters, namely the waist of the microlenses, the working distance, the optimal bending radius and the efficiency of the optical coupling. For this purpose, the experimental set-up dedicated to the characterization is as shown in Fig. 7.

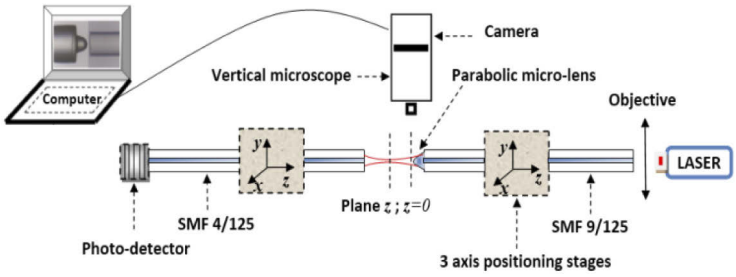

Fig. 7. Experimental set-up for characterizing parabolic microlensed fibers

The set-up is composed first by a laser source (λ = 1,31µm) coupled into a 9/125 fiber with a microlens by a microscope lens (×10). Then, an acquisition system composed of a Charge-coupled device (CCD) camera combined with a vertical microscope is used to control the centering and alignment of the parabolic microlens tip in front of a 4/125 µm "measurement" fiber going to a photo-detector. The latter is used to scan the output beam in both perpendicular directions (***x*** and ***y***) of the transverse plane as well as the axial direction ***z***. The microlens and the measuring fiber are fixed on a 3D micro-displacement system. The nanometric displacement in the z direction is ensured by a piezo-positioner (Edmund PP-30). The longitudinal and transverse translations of the measurement fiber allow to scan the beam profile of the coupling area from the surface of

OPTICS CONTINUUM

the microlens ($z = 0$). The photodetector (InGaAs Photodiode IGA-Series from Edmund optics) gives the value of the coupled light intensity.

At maximum optical coupling, the working distance Z and the image waist w_l were determined. For this reason, five different microlenses were characterized by following the same procedure.

4.2. Results and discussions

The transmitted light intensity was measured in a scanned coupling volume of 12 µm in the transverse plane and 40 µm in the axial direction in 1 µm steps at a resolution of 10 nm. The experimental values were then interpolated by a Gaussian distribution as shown in Fig. 8 (a). These variation curves show the scanned coupling volume. From the longitudinal section of the curves (Fig. 8 (b)), the working distance Z, starting from the surface of the microlens ($z = 0$) to the maximum of the curve, is deduced. From the transverse curve at the minimum width of the coupling volume, in this case at $Z = 21$ µm, the waist of the focus spot is determined.

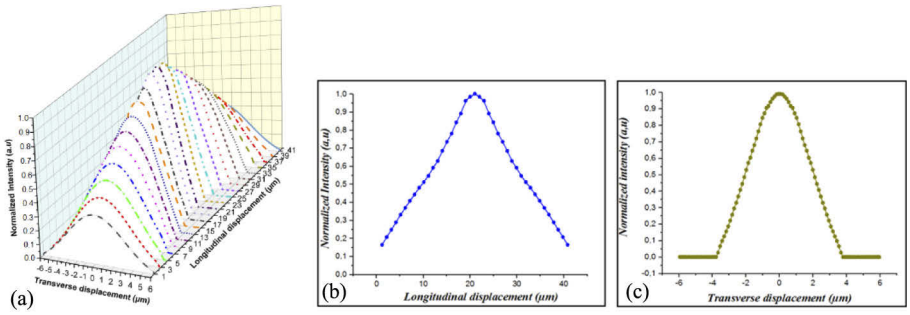

Fig. 8. Coupling between a 9/125 fiber (with microlens) and a 4/125 fiber. (a) Representation of the Gaussian interpolation curves (41) of the experimental values in the coupling volume from z = 21 µm (front curve) to z = 41 µm (back curve). (b) Longitudinal section of the coupling volume. (c) Transversal section at the minimum width of the coupling volume.

In Fig. 8, the measurements concern a single case of microlens. Therefore, in order to optimize the coupling, it is essential to find the optimal microlens bending radius yielding the best performance. The curves (a) and (b) in Fig. 9 show, respectively, the theoretical and experimental curves of the variation of the waist and the working distance as a function of the curvature radius of the parabolic microlenses in PDMS with the index $n_s = 1.418$, integrated on a 9/125 µm single mode fiber at both wavelengths $\lambda = 1.310$ and 1.550 µm. The curves are monotonic within the range of the studied curvature radii (2.5–21 µm). The optimal bending radius corresponds to the maximum coupling value. The coupling coefficient η variation as a function of the microlenses' bending radius is shown in Fig. 9 (c). In this figure, the coupling efficiency curves are normalized with respect to the maximum values. Theoretically $\eta \sim 100\%$ (Eq. 28) for optimal curvature radius $R = 10.08$ µm. However, the experimental values are lower at the closest radius of curvature, i.e. $R = 9.05$ µm (Table 2). That is, a decreasing of 1.4% and 0.7% occurs at the two wavelengths of interest. Therefore, the coupling values are 98% at 1.310 µm and 98.9% at 1.550 µm, respectively Table 2 summarizes the results obtained.

The waist values achieved experimentally varies from 1.0 to ~5.0 µm with working distances from 5.80 to 48.80 µm at λ=1.310 µm. These values are very close to those obtained at λ=1.550 µm. Hence, the most suitable elaborated microlens corresponds to a curvature radius $R_{opt} = 9.50$ µm in terms of coupling efficiency.

Table 2. Characteristics of the Five Different Studied Microlenses (w_f =2.28 µm and λ=1.31 µm).

λ (μm)	at λ=1.310 μm						at λ=1.550 μm						
$R(\mu m)$	$Z_{theo}(\mu m)$		$w_{ltheo}(\mu m)$	$w_{lexp}(\mu m)$		η_{exp}(%)		$Z_{theo}(\mu m)$	$Z_{exp}(\mu m)$	$w_{ltheo}(\mu m)$	$w_{lexp}(\mu m)$		η_{exp}(%)
2.50	6.32	5.80	1.09	1.00	44.85	34.04	07.60	06,06	1,25	1,07	47,10	39,20	
9.50	23.41	22.95	2.30	2.12	<100	98.03		24.75	23,18	2,48	2.27	100	98.90
13.50	34.80	34.00	3.35	3.06	97.02	95.82		36.20	34,40	3,51	3.24	98,85	96.88
17.50	44.80	43.90	4.39	3.98	89.80	86.26		46.19	44,36	4,52	4.18	91,01	88.15
21.00	49.68	48.80	5.08	4.86	78.71	76.90		50.98	49,30	5,28	5.19	81,05	79.55

OPTICS CONTINUUM

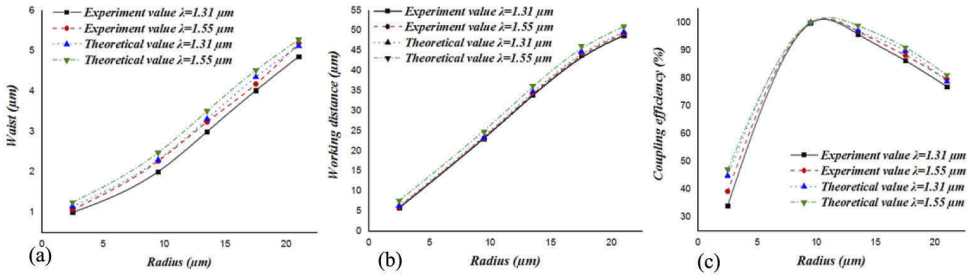

Fig. 9. Theoretical and experimental curves, provided simultaneously at λ =1.31 and 1.550 μm, corresponding to (a) the waist, (b) the working distance, (c) the coupling efficiency, as a function of the microlenses' curvature radius.

5. Conclusion

The aim of this work was to optimize optical coupling where aberrations induced by spherical microlenses are present. The theoretical and experimental performances of microlenses with parabolic microlenses had been studied in details. The microlenses' profile was determined using image processing by extracting their contours. The interpolation of the points allowed the determination of the curvature radius at the apex and an estimate on the aberration coefficient. The results have shown that, at the two relevant wavelengths, there would be 64% and 68% reductions in aberrations if used, respectively, parabolic and hyperbolic microlenses. These also would lead to a spot size reduction. As a result, optical coupling to most other components can be improved. In this regard, the coupling efficiency was also optimized with respect to the microlenses bending radius. Among the five microlenses undertaken, the maximum coupling is attained for $R_{opt} = 9.50\,\mu m$ which is close to the maximum theoretical predicted value $R = 10.08\,\mu m$. It is worth mentioning that the microlenses were characterized on a special experimental bench where the coupling zone was analyzed in a volume axially greater than the Rayleigh distance. At maximum coupling, the main optical parameters were determined namely the waist, the working distance and the coupling rate. The results presented herein, as far as the performance is concerned, are in favor of the use of parabolic microlenses. These optical components can find suitable applications in optical connections and near-field surface analysis.

Funding. General Directorate of Scientific Research and Technological Development (DGRSDT); Ministry of Higher Education and Scientific Research (MESRS) (D01220140058).

Acknowledgments. This work was supported by the General Directorate of Scientific Research and Technological Development (DGRSDT), Ministry of Higher Education and Scientific Research (MESRS), Algeria (Project number D01220140058). The authors also want express their gratefulness to Amandine Elchinger (Unistra) and Pr. Ameur Zegadi (UFAS) for the neat writing and helpful comments.

Disclosures. The authors declare no conflicts of interest.

Data availability. No data were generated or analyzed in the presented research.

References

1. J. Kim, M. Han, S. Chang, Jhang W. Lee, and K. Oh, "Achievement of Large Spot Size and Long Collimation Length Using UV Curable Self-Assembled Polymer Lens on a Beam Expanding Core-Less Silica Fiber," IEEE Photonics Technol. Lett. **16**, 2499–2501 (2004).
2. X. Zhou, Z. Chen, Z. Wang, and J. Hou, "Monolithic fiber end cap collimator for high-power free-space fiber–fiber coupling," Appl. Opt. **55**(1), 4001 (2016).
3. M. Zaboub, A. Guessoum, N.E. Demagh, and A. Guermat, "Fabrication of polymer microlenses on single mode optical fibers for light coupling," Opt. Commun. **366**, 122–126 (2016).
4. K. Shiraishi and S-I Kuroo, "A new lensed fiber configuration employing cascaded Gi-fiber chips," J. Lightwave Technol. **18**(6), 787–794 (2000).

OPTICS CONTINUUM

5. S.H. Ghasemi, M. R. Hantehzadeh, J. Sabbaghzadeh, D. Dorranian, V. Vatani, A. Babazadeh, K. Hejaz, A. Hemmati, and M. Lafouti, "Designing plano-convex aspheric lens for fiber optics collimator," Opt. Lasers Eng. **50**(2), 293–296 (2012).
6. J.C. Tsai, M. F. Chen, and H. Yang, "Design and Fabrication of High Numerical Aperture and Low Aberration Bi-Convex Micro Lens Array," DTIP 9–11 (2008).
7. J.Y Hu, C.P. Lin, S.Y. Hung, H. Yang, and C.K. Chao, "Semi-ellipsoid microlens simulation and fabrication for enhancing optical fiber coupling efficiency," Sens. Actuators, A **147**(1), 93–98 (2008).
8. F. A. Rahman, K. Takahashi, and C. H. Teik, "Theoretical analysis of coupling between laser diodes and conically lensed single-mode fibres utilizing ABCD matrix method," Opt. Commun. **215**(1-3), 61–68 (2003).
9. S. D. Alaruri, "Single-mode fiber-to-single-mode fiber coupling efficiency and tolerance analysis: comparative study for ball, conic and GRIN rod lens coupling schemes using Zemax Huygen's integration and physical optics calculations," Optik (Munich, Ger.) **126**(24), 5923–5927 (2015).
10. S. Gangopadhyay and S. Sarkar, "ABCD matrix for reflection and refraction of Gaussian light beams at surfaces of hyperboloid of revolution and efficiency computation for laser diode to single-mode fiber coupling by way of a hyperbolic lens on the fiber tip," Appl. Opt. **36**(33), 8582–8586 (1997).
11. C. H. Tien, Y. C. Lai, T. D. Milster, and H.P.D. Shieh, "Fiber-Lens-based Module for Optical Recording Applications," J. Appl. Phys. **41**(Part 1, No. 3B), 1834–1837 (2002).
12. A.K. Das, A.K. Ganguly, and A. Saha, "Multi - layered step index micro - lens of low spherical aberration," SPIE **3557**, 0277–786X (1998).
13. M. Thual, G. Moreau, J. Ribette, P. Rochard, M. Gadonna, and J.C. Simon, "Micro-Lens on Polarization Maintaining Fibre for Coupling with 1.55µm Quantum Dot Devices," Opt. Commun. **255**(4-6), 278–285 (2005).
14. S.D. Le, E. Delcourt, P. Girault, A. Gutierrez, P. Azuelos, N. Lorrain, L. Bodiou, L. Poffo, J.M. Goujon, Y. Dumeige, I. Hardy, P. Rochard, J. Lemaitre, P. Pirasteh, M. Guendouz, T. Chartier, L. Quétel, S. Claudot, J. Charrier, and M. Thual, "Study of Optimized Coupling Based on Micro-Lensed Fibers for Fibers and Photonic Integrated Circuits in the Framework of Telecommunications and Sensing Applications," Commun. Phys. (Hanoi, Viet Nam) **26**(4), 325 (2017).
15. R. Pierron, G. Chabrol, S. Roques, P. Pfeiffer, J-P. Yehouessi, G. Bouwmans, and S. Lecler, "Large-Mode-Area Optical Fiber for Photonic Nanojet Generation," Opt. Lett. **44**, 2474 (2019).
16. H. Z. Liu, "The approximate matrix for a parabolic lens of revolution and its application in calculating the coupling efficiency," Optik **119**(14), 666–670 (2008).
17. S. Lecler, N. E. Demagh, A. Guessoum, D. Bouaziz, and Z. Bouhafs, "Process and system for manufacturing an optical component by moulding an optical fiber," EPO – Patent **21315008**, 9–1001 (2021).
18. D. Marcuse, "Loss analysis of single-mode fiber splices," Tech. J. **56**, 703–718 (1977).
19. S. Mukhopadhyay, "Coupling of a laser diode to single mode circular core graded index fiber via parabolic microlens on the fiber tip and identification of the suitable refractive index profile with consideration for possible misalignments," J. Opt. **45**(4), 312–323 (2016).
20. M. Do Carmo, "Differential geometry of curves and surfaces," Prentice Hall, (1976).
21. W. Emkey and C. Jack, "Analysis and evaluation of graded-index fiber lenses," J. Lightwave Technol. **5**(9), 1156–1164 (1987).
22. S. Vazquez-Montiel and O. Garcıa-Lievanos, "Spherical aberration correction using aspheric surfaces with an analytic-numerical method," Rev. Mex. Fis. **59**, 273–281 (2013).
23. D Mcister, Aspheric lenses: optics and applications Lens Talk, 26(25), (1998).
24. Ph. Nussbaum, R. Volkely, H. P. Herzig, M. Eisner, and S. Haselbeck, "Design, fabrication and testing of microlens arrays for sensors and Microsystems," Appl. Opt. **6**, 617–636 (1997).
25. H. P. Herzig, ed., (1997) *Micro-optics* (Taylor and Francis: London)
26. H. Naumann and G. Schroeder, (1992) *Bauelemente der Optik* (Munich: Hanser)
27. S. N. Sarkar, B. P. Pal, and K. Thyagarajan, "Lens Coupling of Laser Diodes to Monomode Elliptic Core Fibers," J. Opt. Commun. **7**(3), 92–96 (1986).
28. W.B. Joyce and B.C. DeLoach, "Alignment of Gaussian beams," Appl. Opt. **23**(23), 4187–4196 (1984).